A. Kawasaki and J. Kasahara, A novel characteristic length of detonation relevant to supercritical diffraction, SHOCK WAVES, Vol. 30, No. 1, 2020, pp. 1-12

Title **A Novel Characteristic Length of Detonation Relevant to Supercritical Diffraction**

Authors Akira Kawasaki and Jiro Kasahara

Affiliation Department of Aerospace Engineering, Nagoya University
Furo-cho, Chikusa-ku, Nagoya, Aichi 464-8603, Japan

Corresponding author's contact information Jiro Kasahara
E-mail: kasahara@nuae.nagoya-u.ac.jp
Phone: +81-52-789-4404

ORCID Akira Kawasaki 0000-0003-4532-3682
Jiro Kasahara 0000-0002-6524-1345

Abstract For stoichiometric C_2H_4–O_2 and C_2H_2–O_2 mixtures with or without argon dilution, the processes of detonation diffraction have been investigated in a two-dimensional setup through high-speed schlieren imaging, with the characteristic length and the stability of detonation varied by regulating the initial pressure and argon mole fraction of the mixture. In particular, a length relevant to the process of supercritical diffraction (i.e., distance from the channel end corner to reflection point of the transverse detonation on the channel end face, reflection point distance in short) was deduced from obtained sequential schlieren images and analyzed. The reflection point distance can be idealized for the infinitely wide donor channel, and thus it can be an parameter in which properties intrinsic to each detonable mixture are manifested. Experimental results showed that the reflection point distance was roughly inversely proportional to the initial pressure for identical mixtures and independent of the width of the donor channel at high initial pressures. For a certain combination of the fuel and oxidizer, correlations between the reflection point distance and the initial partial pressure of fuel were very similar regardless of the argon mole fraction. Critical conditions of the diffraction problem could be given for the ratio of the reflection point distance to the channel width, and it was suggested that the critical value lies in a range of 3–5 and does not significantly depend on the stability of the mixture.

Keywords Reflection point distance, Detonation dynamic parameters, Detonation diffraction, Critical tube diameter, Detonation stability, Schlieren imaging

Acknowledgments The authors thank Ken Matsuoka and Akira Iwakawa for fruitful discussions. This research was financially supported by the Nitto Foundation and the Japanese Society for the Promotion of Science (JSPS) KAKENHI Grant Number 17H06741, 17H03480, and 17K18937.

List of symbols

D_{CJ}	Chapman–Jouguet (CJ) velocity
d_{dt}	Diameter of detonation tube
E_a	Activation energy
p_0	Initial pressure of mixture
$p_{0,f}$	Initial partial pressure of fuel
l_c	Channel width
l_r	Reflection point distance
R	Universal gas constant
T_0	Initial temperature
T_{vN}	von Neumann temperature
t_{oc}	Depth of observation chamber
y_{Ar}	Argon mole fraction
Δ_i	Induction length
λ	Detonation cell width
τ_i	Induction time
τ_r	Reaction time

41 χ Detonation stability parameter

42

43 ## 1. Introduction

44 When a planar detonation wave propagating in a channel emerges into a wider space, the wave front
45 undergoes deformation and diffraction due to expansion of the flow behind the leading shock wave. The
46 transmission of the detonation from the channel into the wider space can fail under certain conditions. Based on
47 success or failure in the transmission, the diffraction process is often classified as supercritical or subcritical,
48 respectively [1], and there exists a critical condition for the size of the channel, depending on the configuration of
49 the channel and the composition and thermodynamic states of the detonable gas mixture [1, 2]. For instance,
50 Zel'dovich *et al*. [3] pointed out that a detonation wave in a cylindrical tube will fail in transmission upon
51 diffraction when the diameter of the tube is smaller than a certain value, which is called the critical tube diameter.

52 The critical tube diameter is a measure of the detonability of combustible mixtures [4, 5] and known as a
53 typical dynamic parameter of detonation phenomena, although quantitatively predictive theory for the critical tube
54 diameter is still under development [4]. The critical tube diameter has often been discussed in relation to the
55 detonation cell size in order to predict its value. However, the relationship between the critical tube diameter and
56 detonation cell width is not completely universal. The relationship depends on the geometry of the flow field and
57 the stability of the mixture. Mitrofanov and Soloukhin [6] discovered that, for the stoichiometric acetylene-oxygen

mixture at low pressures, the critical diameter is 13 or 10 times the cell width for a cylindrical tube where the flow field is three-dimensional and a thin rectangular channel where the flow field is two-dimensional, respectively. Later, the correlation between the critical tube diameter and cell width was confirmed for wider ranges of the initial pressure and wider variety of fuel-oxidizer mixtures and channel geometry in other works [7–13]. This correlation, however, was found not to hold for more stable mixtures with regular cellular patterns, including mixtures with high argon dilution; instead, larger numbers of cells are required for a planar detonation wave to successfully transmit from a channel into unconfined space [14–17]. Although the theoretical aspect of the correlation between the critical channel size and the cell width remains an open problem, differences in the manner of the correlation among mixtures with different stabilities are associated with the differences in the failure mechanisms of detonation transmission [2, 4, 18–20].

Hence, many experiments and numerical simulations have been done to investigate the process of detonation diffraction in detail. In an experiment by Bartlmä and Schröder [21], high-time-resolution sequential schlieren photographs were obtained for processes of supercritical diffraction (success in transmission) and subcritical diffraction (failure in transmission) using a multi-spark optical system. Based on the observations, they concluded that re-initiation and formation of a transverse detonation are necessary for successful detonation transmission. Jones *et al*. [22] performed two-dimensional numerical simulations to investigate the influences of the cellular structure on the diffraction process. They concluded that transverse waves are necessary for re-initiation of the

detonation, and the number of the transverse waves are also important because successive propagation of the transverse waves leads to a local explosion and subsequent transverse detonation. Pintgen and Shepherd [23] examined the influence of the detonation stability on the features of diffraction through simultaneous schlieren imaging, chemiluminescence imaging, and laser-induced fluorescence (LIF) imaging of OH radicals. In that study, they found that, in subcritical diffraction processes, the detonation velocity on the symmetrical axis for a more stable mixture (hydrogen–oxygen–argon mixture) decays significantly slower than for a more unstable mixture (hydrogen–nitrous oxide mixture), whereas, in supercritical diffraction processes, the re-initiation events appeared similar for the two mixtures. In recent years, Deiterding [24] and Li *et al*. [25] performed high-resolution numerical simulations based on the inviscid, reactive Euler equations. In the simulations, cell-scale physics were resolved by means of adaptive mesh refinement (AMR) and parallel computing, and the reproduced critical conditions between channel width and cell size were quantitatively consistent with experiments. Mehrjoo *et al*. [26, 27] examined the influence of cellular instability on detonation diffraction by perturbing the flow behind the leading shock with obstacles or porous walled tubes. In the experiments, for more stable mixtures with high argon dilution, the critical condition between the tube and cell sizes was not significantly affected, whereas for unstable mixtures, the critical condition was significantly changed.

On the other hand, another correlation regarding the detonation diffraction problem is also becoming evident for the reflection point distance of transverse detonation, which is the distance on a tube end face between the tube

92 end corner and a point where a detonation wave reattaches by re-initiation. Murray and Lee [28] discovered a
93 circular pattern on a soot foil on the tube end wall for equimolar acetylene-oxygen mixtures, and they found that
94 the distance between the circular pattern and the tube inner wall, which is equivalent to the reflection point distance,
95 was well correlated with detonation cell width. Nagura *et al*. [29, 30] also concluded that the reflection point
96 distance is roughly proportional to the detonation cell width for stoichiometric ethylene-oxygen and
97 acetylene-oxygen mixtures. These facts are exceptionally important, because if there exists some correlation
98 between reflection point distance and cell width, it would mean that reflection point distance, which can be easier
99 to measure, is equivalent to the cell width.

100 In the present study, for stoichiometric ethylene-oxygen and acetylene-oxygen gas mixtures, we investigated
101 processes of detonation diffraction through high-speed schlieren imaging in a two-dimensional setup with the initial
102 pressure and argon dilution ratio of the mixture varied. Based on the obtained sequential schlieren images, the
103 reflection point distance relevant to the supercritical diffraction process was deduced and examined as a
104 characteristic length of detonation.

105

106 ## 2. Experimental Setup

107 ### 2.1. Experimental apparatus

108 The experimental apparatus consisted mainly of an observation chamber, detonation tube, dump tank, and
109 schlieren imaging system. A schematic of the observation chamber is shown in Fig. 1. The observation chamber

was connected to the detonation tube on the lower side, and with the dump tank in the downstream direction. In an operation, a planar detonation wave generated in the detonation tube was introduced into the observation chamber through an inlet channel from the lower side. The planar detonation wave then experienced an abrupt expansion at the end of the inlet channel and was diffracted toward the upper right within the rectangular diffraction region. Note that the flow-fields obtained in the present setup can be regarded as right halves of symmetric flow-fields in cylindrical diffraction; the vertical wall of the observation chamber corresponds to the line of symmetry. Once the detonation wave reached a diaphragm inserted at the joint between the observation chamber and the dump tank, the diaphragm was ruptured, and the high temperature and pressure burnt gas was safely released into the dump tank. During this sequence of events, the process of detonation diffraction occurring within the observation chamber was visualized by the schlieren method and recorded with a high-speed video camera.

The observation chamber, consisting of inlet and outlet channels and a diffraction region, had a structure uniform in depth between two parallel optical windows. The gap between the optical windows was t_{oc} = 16 mm, which was significantly greater than the detonation cell widths at the conditions of interest, thus transverse waves in depth were not suppressed. The inlet channel was 90-mm long and had a rectangular cross-section with a width of l_c = 10 or 20 mm (variable) and a depth of t_{oc}; the aspect ratio of the cross-section was thus t_{oc}/l_c = 1.6 or 0.8, respectively. However, regardless of the aspect ratio, the diffraction taking place in the present setup was cylindrical (two-dimensional) but not spherical (three-dimensional) because the flow was bounded by the parallel

windows. Note that this situation is equivalent to the case of the infinite aspect ratio in unbounded, fully open space [11]. The dimensions of the diffraction region were 60 mm in length, 80 mm in width, and t_{oc} in depth, and the depth is identical with the inlet channel. The detonation tube had a length of 560 mm and a circular cross-section with an inner diameter of d_{dt} = 25.8 mm, and also was equipped with a Shchelkin spiral at the bottom. The diaphragm separating the observation chamber from the dump tank was made of 12-μm thick polyester. Before operation, the detonation tube, observation chamber, and dump tank were well evacuated by an oil-sealed rotary pump. Once the apparatus was evacuated, the detonation tube and observation chamber were filled with a fuel-oxidizer mixture, prepared by a mixing tank. A spark plug installed at the bottom end of the detonation tube was used to ignite the mixture.

The schlieren optical system consisted of a low-coherence, diode-laser light source (Cavitar/CAVILUX), a high-speed charge-coupled device (CCD) video camera (Shimadzu/HPV-1), and some optical elements. A 150-mm diameter convex lens with a 450-mm focal length was used to collimate the light emitted from the source. The parallel rays of light were exposed to the observation chamber, and condensed again by a 200-mm diameter concave mirror with a focal length of 1500 mm. A knife edge was positioned horizontally at the focus of the concave mirror. Flashes of the light source were synchronized with exposures of the camera. The camera was triggered by a pulse generator based on the signal of a pressure sensor installed in the observation chamber. The emission time of the light source was set to 30 ns, and the camera exposure time was set to 250 ns. As described

below, typical propagation speed of the detonation waves D_{CJ} was approximately 2000 m/s for the conditions in this study; the blur of the detonation front in an image could be suppressed down to 60 μm due to the short emission time of the light source. The influence of self-luminescence was also suppressed due to the short exposure time. The frame interval was set to 1 or 2 μs, depending on the mixture, and typical displacement of the detonation fronts between frames could be estimated as 2 or 4 mm for D_{CJ} = 2000 m/s. The spatial resolution of the obtained images was approximately 0.3 mm.

2.2. Experimental conditions

Experimental conditions and typical mixture characteristics are listed in Table 1. In the present study, ethylene or acetylene gas, oxygen gas, and argon gas were employed for fuel, oxidizer, and diluent, respectively. As shown in Table 1, four types of stoichiometric ethylene–oxygen mixtures (E1–E4) were prepared with a variation of argon mole fraction y_{Ar}, as well as two types of stoichiometric acetylene–oxygen mixtures (A1–A2). For the ethylene-oxygen mixture without argon dilution (E1), the inlet-channel width l_c of the observation chamber was varied. Initial pressure (filling pressure) of the mixtures p_0 ranged from 5–140 kPa, and initial temperature T_0 was at room temperature (22±6 ˚C). In the present study, we focused particularly on two parameters that characterize mixtures. The first was the characteristic length of detonation, and the second was detonation stability. The characteristic length of detonation was varied by controlling the initial pressure of the mixture; detonation stability

was varied by changing the argon mole fraction of the mixture.

To clarify the characteristics of the mixtures, Chapman–Jouguet (CJ) detonation velocities and stability parameters were calculated for the seven mixtures for a representative initial condition such that p_0 = 50 kPa and T_0 = 22˚C, as shown in Table 1. The CJ velocity was calculated using the NASA CEA code [31, 32]. As shown in Table 1, CJ detonation velocity D_{CJ} decreases with an increase in the argon mole fraction y_{Ar} for the ethylene and acetylene mixtures. This is the result of the lowering of exothermicity, which drives detonation. That is, in a more highly diluted mixture, heat release per unit mass of the mixture decreases because of the decrease in the mass fraction of the fuel. Additionally, as shown in Table 1, comparing the E1 and A1 mixtures and E4 and A2 mixtures, it is evident that differences in CJ velocity due to the difference in fuel species is minor for similar argon mole fractions.

Although some parameters have been proposed to parameterize the detonation stability of the mixture, in the present study, the χ parameter computed as follows was used as a stability parameter in accordance with reference [33].

$$\chi = \frac{\tau_{\mathrm{i}}}{\tau_{\mathrm{r}}}\frac{E_{\mathrm{a}}}{RT_{\mathrm{vN}}}, \tag{1}$$

where τ_{i} refers to induction length, τ_{r} is reaction length, E_{a} is overall activation energy, R is the gas constant, and T_{vN} is the von Neumann pressure. The stability parameter was evaluated based on a solution of the Zel'dovich-von Neumann-Döring (ZND) model simulation [34] with the GRI-Mech 3.0 chemical reaction model [35]. The

177 induction time was computed as the arrival time interval of the leading shock and the maximum-thermicity point.
178 The reaction time was computed as the inverse of the maximum thermicity. The activation energy was computed in
179 accordance with the method described in Reference [23]. As shown in Table 1, with an increase in the argon mole
180 fraction, the stability parameter decreased from the order of 10^1 and approached the order of 10^0 for the ethylene
181 and acetylene mixtures. Note that in the case of the E4 mixture, a highly regular cell pattern was obtained in
182 Reference [36].

183 For each mixture, a correlation equation between the initial pressure and the cell width was derived in
184 reference to existing experimental data, e.g., in the CALTECH detonation database [37]. The equations are as
185 follows;

$$\lambda_{\mathrm{E1}} = 72.87 \times p_0^{-1.136} \quad \text{for the E1 mixture;} \tag{2}$$

$$\lambda_{\mathrm{E2}} = 97.96 \times p_0^{-1.140} \quad \text{for the E2 mixture;} \tag{3}$$

$$\lambda_{\mathrm{E3}} = \sum_{j\in\{\mathrm{E1,\,E2,\,E4}\}} \lambda_j \prod_{\substack{k\in\{\mathrm{E1,\,E2,\,E4}\}\\ k\neq j}} \frac{y_{\mathrm{Ar,E3}} - y_{\mathrm{Ar},k}}{y_{\mathrm{Ar},j} - y_{\mathrm{Ar},k}} \quad \text{for the E3 mixture;} \tag{4}$$

$$\lambda_{\mathrm{E4}} = 160.9 \times p_0^{-1.066} \quad \text{for the E4 mixture;} \tag{5}$$

$$\lambda_{\mathrm{A1}} = 23.64 \times p_0^{-1.033} \quad \text{for the A1 mixture;} \tag{6}$$

$$\lambda_{\mathrm{A2}} = 386.3 \times p_0^{-1.244} \quad \text{for the A2 mixture,} \tag{7}$$

186 where λ_{E1} to λ_{A2} are in mm and p_0 is in kPa. Except for the E3 mixture, the equations were derived directly by
187 performing the power-law best fit. For the E3 mixture, the equation was developed by Lagrange interpolation from

188 the equations for the E1, E2, and E4 mixtures because experimental data were not available. The equation number

189 and detailed references corresponding to each mixture are listed also in Table 1.

190

191 ## 3. Results and Discussion

192 ### 3.1. Diffraction process

193 Figure 2 present representative results of the sequential schlieren imaging, supercritical and subcritical

194 detonation processes for the stoichiometric ethylene-oxygen mixture without argon dilution (E1), and a channel

195 width l_c of 10 mm, with a frame interval of 2 μs. The order of the photographs corresponds to the time evolution of

196 the processes. Note that the sequences of schlieren photographs were obtained for single diffraction events.

197 The supercritical diffraction process shown in Fig. 2 (a) (and Movie 1a, available as supplementary material)

198 was obtained for the conditions of the mixture where initial pressure and temperature were 30 kPa and 20 °C,

199 respectively. Note that the images were originally obtained with a frame interval of 1 μs, but that some were

200 omitted because of space limitations. In Fig. 2 (a-1), a planar detonation wave generated in the detonation tube can

201 be observed in the inlet channel. The detonation wave then reached the end of the inlet channel and experienced the

202 abrupt expansion of the channel between Figs. 2 (a-1) and (a-2). After emerging into wider space (Figs. 2 (a-1) –

203 (a-5)), the detonation wave front underwent deformation gradually, due to the expansion waves generated at the end

204 corner of the inlet channel. Particularly in the vicinity of the horizontal wall, the reaction front was decoupled from

205 the shock front, whereas coupling of the shock front and reaction front was retained in the vicinity of the vertical

wall, as shown in Figs. 2 (a-2) – (a-9). This behavior has been interpreted as transverse waves accompanying the detonation front being more significantly attenuated in the vicinity of the horizontal wall by the expansion waves generated at the end corner of the inlet channel. In Fig. 2 (a-6), a bulge can be observed at the upper-right part of the detonation front, which is an indication of a local explosion, i.e., re-initiation of the transverse detonation. In Figs. 2 (a-6) – (a-9), the bulge evolved into a transverse detonation wave that swept the shocked but unreacted region, i.e., the region between the decoupled shock and reaction fronts, toward the horizontal wall. Finally, the transverse detonation wave reached the horizontal wall, as shown in Fig. 2 (a-10). At this point, the detonation wave front that had detached from the horizontal wall temporarily upon emergence into the wider space reattached to that wall. Later, in Figs. 2 (a-11) and (a-12), the transverse detonation wave was reflected on the wall.

As mentioned in the Introduction, it is known that the locus of reflection of the transverse detonation on the horizontal wall behaves in an orderly way [2, 23, 28]. Thus, in the present study, we redefine the distance between the reflection point of the transverse detonation wave and the end corner of the inlet channel as a novel characteristic length of detonation phenomena, and we refer to it as the *reflection point distance* l_r. How to determine the locus of reflection of the transverse detonation is examined in more depth below, in conjunction with the reflection event.

Figure 2 (c) shows schematic illustrations of the temporal development of a reflection event in a process of supercritical diffraction. The illustrations were rendered based on the schlieren images obtained for the same

operation shown in Fig. 2 (a). In the process of supercritical diffraction, the point of intersection between the transverse detonation wave and the decoupled shock front arose after a local explosion, as shown in Figs. 2 (a-8) and Fig. 2 (c-1). The point of intersection moved along the decoupled shock front with the propagation of the transverse detonation until finally reaching the horizontal wall, as shown in Figs. 2 (a-9) and (a-10). Thus, a reflection point distance l_r was quantified based on a high-speed schlieren image as the distance from the exit corner of the channel to the locus where the intersection arrives at the horizontal wall, as shown in Fig. 2 (c-2). Here, the pressure distribution is thought to have a locally maximum value at the point of intersection between the transverse detonation and decoupled shock front. Thus, the reflection point distance defined above corresponds to the circular patterns in the soot foil records on the exit face described in [28], which can be interpreted as the history of the locus of locally highest pressure. In the following subsection, we consider the characteristics of the reflection point distance.

The subcritical diffraction process shown in Fig 2 (b) (and Movie 1b, available as supplementary material) was obtained for the conditions of the mixture where the initial pressure and temperature were 10 kPa and 20 °C, respectively. In Fig. 2 (b-1), as in the supercritical case, a planar detonation wave can be observed in the inlet channel. Between Figs. 2 (b-1) and (b-2), the detonation wave emerged into wider space. The expansion wave was then generated at the end corner of the inlet channel, and similarly propagated leftward while the detonation wave front underwent deformation, as shown in Figs. 2 (b-2) – (b-6). Over the course of these figures, in contrast to the

supercritical case, the expansion waves attenuated the transverse waves accompanying the detonation front more significantly, and the reaction front was immediately decoupled from the shock front upon the passing of the head of the expansion waves.

By the time of Fig. 2 (b-7) or (b-8), the head of the expansion fan reached the vertical wall, and the reaction front totally decoupled from the shock front. The quenching mechanism in this case can be classified into the local quenching mode described by Lee [1]. After Fig. 2 (b-8), the shock front was decelerated, which can be observed by comparing Fig. 2 (b) to 2 (a). That is, from Figs. 2 (b-1) to (b-6) or (b-7), the locus of the detonation front on the vertical wall coincides with the one observed in Figs. 2 (a-1) to (a-6) or (a-7), whereas after Fig. 2 (b-8), the difference in the loci of the detonation front becomes evident. Additionally, in Figs. (b-4) – (b-12), attenuated transverse wave remnants can be observed, and the spacing between them expands with time.

3.2. Reflection point distance

Before entering into the details of the results , the nature of the reflection point distance is briefly discussed here. The reflection point distance should be essentially defined in a system with an infinitely wide donor channel. In such an ideal system, there is no length scale characterizing the geometry, and thus the features of the flow-field are determined based only on physical and chemical properties intrinsic to the mixture [49]. That is, in such a system, the reflection point distance can be a characteristic length manifesting a property of the detonable mixture.

In the present experiments, in reality, the channel width must be, of course, finite, and thus the wall of the channel affects the flow-field by reflecting transverse waves of the detonation and the rarefaction wave generated at the corner of the channel. However, by using a wide enough donor channel compared to the transverse wave spacing of the detonation wave, influence of the physical boundary is expected to be suppressed. Hence, at high initial pressures where the transverse wave spacing is small, the reflection point distances obtained in experiments are substantially equivalent to the ideal ones, aside from the inherent variation arising from the stochastic nature of the detonation diffraction problem.

In Figs. 3 and 4, as a summary of data reduction results from the schlieren images, reflection point distance l_r as a function of the initial pressure p_0 of the mixture is shown in a double-log scale for the stoichiometric ethylene-oxygen mixtures (E1–E4) with different argon mole fraction y_{Ar}, as well as the stoichiometric acetylene-oxygen mixtures (A1–A2). The circles correspond to the ethylene mixtures (E1–E4), and the squares to the acetylene mixtures (A1–A2). The sizes of the symbols correspond to the argon mole fraction y_{Ar}, i.e., the smaller the symbol, the more highly diluted the mixture. The closed symbols refer to the case where channel width l_c = 10 mm, whereas the open symbols indicate the case where channel width l_c = 20 mm. The dashed auxiliary lines indicate inversely proportional relations as an aid in visualization.

Based only on Fig. 3, we describe the influence of the initial pressure p_0, argon mole fraction y_{Ar}, and channel width l_c, focusing on the ethylene mixtures (E1–E4). For constant argon mole fractions, the reflection point

distance l_r decreases with the increase in the initial pressure of the mixture. The relations between the reflection point distance and the initial pressure appear to be roughly inversely proportional, although slight deviations can be seen at low pressures (e.g., y_{Ar} = 0 %, l_c = 20 mm, and p_0 = 15 kPa). This deviation can be attributed to the fact that the channel width was not sufficiently wider than the transverse wave spacing at those initial pressures. For constant initial pressures, the reflection point distance increases with the argon mole fraction; e.g., in Fig. 3, at l_c = 10 mm and p_0 = 50 kPa, l_r = 11.2, 23.9, and 41.2 mm for y_{Ar} = 0 %, 50%, and 67%, respectively. The argon mole fraction also seems to affect the scattering of the reflection point distance. Namely, the scattering of the reflection point distance becomes more significant as the argon mole fraction increases. Additionally, for the E1 mixture (y_{Ar} = 0 %), the reflection point distance appears to be not significantly influenced by the change in the channel width, and reflection point distances are similar for both the channel widths (l_c = 10 and 20 mm), particularly at high initial pressures. This fact suggests that the channel is wide enough, and reflection point distances obtained at such high initial pressures are close to the ideal ones.

By comparing Figs. 3 and 4, the influence of the fuel species can also be deduced. First, descriptions of the influences of the initial pressure and argon mole fraction for the ethylene mixtures (E1–E4) above are also applicable to the acetylene mixtures (A1–A2). Second, for identical initial pressure, argon mole fraction, and channel width, the reflection point distance is smaller for the non-diluted stoichiometric acetylene-oxygen mixture (A1) than for the non-diluted stoichiometric ethylene-oxygen mixture (E1), e.g., at p_0 = 50 kPa, y_{Ar} = 0%, and l_c =

10 mm, l_r = 2.9 and 11.2 mm for the acetylene mixture and ethylene mixture, respectively.

As another quantity relevant to supercritical diffraction, re-initiation distance has been also discussed, e.g., by Edwards *et al*. [8], Nagura *et al*. [30], and Gallier *et al*. [50]. When a re-initiation distance is defined as a distance between a re-initiation point and the channel end face, the re-initiation distance was approximately 60–90% of the reflection point distance in this study. Additionally, the behavior of the re-initiation distance was similar to the behavior of the reflection point distance. Namely, the re-initiation distance was again roughly inversely proportional to the initial pressure of the mixture and independent of the channel width; with diluent (argon) mole fraction, the re-initiation distance increased and its scattering was enhanced; the re-initiation distance was smaller for the non-diluted acetylene mixture A1 than for the non-diluted ethylene mixture E1 under an identical initial pressure, an argon mole fraction, and a channel width. It is, however, not easy to define the re-initiation distance in an objective fashion depending on a clear criterion because the very onset of the re-initiation is difficult to identify by the method employed in this study. Thus, the following discussion focuses only on the results for the reflection distance.

In Figs. 5 and 6, the reflection point distance l_r as a function of the initial partial pressure of the fuel $p_{0,f}$ for the ethylene mixtures (E1–E4) and acetylene mixtures (A1–A2), respectively, are shown in a double log-scale. The circles correspond to the ethylene mixtures (E1–E4), and the squares to the acetylene mixtures (A1–A2). A smaller symbol corresponds to a more highly argon-diluted mixture. The closed and open symbols refer to the cases where

channel width l_c = 10 and 20 mm, respectively. In the figures, dashed lines represent the best-fit curves obtained by assuming that the reflection point distance l_r is inversely proportional to the initial partial pressure of the fuel $p_{0,f}$. The fitting parameters were the proportionality constants, i.e., the product of the reflection point distance and initial partial pressure of the fuel, $l_r p_{0,f}$. Note that the fitting was performed only for the results which satisfy $l_r/l_c < 4$ because, as mentioned above, the reflection point distance obtained in the experiment is substantially equivalent to the ideal value at high enough initial pressures. Judging from the results shown in Figs. 3 and 4, this criterion seems plausible, albeit somewhat arbitrary. The determined proportionality constants are also shown in the figures. Additionally, in Fig. 7, the determined proportionality constants vs. the argon mole fractions are summarized for the ethylene and acetylene mixtures. The circles correspond to the ethylene mixtures (E1–E4), and the squares to the acetylene mixtures (A1–A2). A smaller symbol corresponds to a more highly argon-diluted mixture. Note that only one fitting curve is provided for the E1 mixture in Fig. 5, although there is a variation in the channel width, because the influence of the channel width on the reflection point distance is minor, as described above.

As can be seen in Figs. 5 and 6, for identical combinations of fuel and oxidizer, the relationship between reflection point distance l_r and initial partial pressure of fuel $p_{0,f}$ is roughly identical, although the reflection point distance tends to increase slightly with the argon mole fraction for the same initial partial fuel pressure. Here, it is also evident that the fitted curves with function forms where reflection point distance is inversely proportional to initial partial pressure of fuel correspond well to the relationship between reflection point distance l_r and initial

partial fuel pressure $p_{0,f}$. As shown in Fig. 7, the proportionality constant slightly increases with the argon mole fraction. Additionally, the constant is smaller for acetylene mixtures than for the ethylene mixtures. The rough identity of the reflection point distance as a function of the initial partial pressure of fuel among different argon mole fractions means that the reflection point distance is determined mainly by the amount of heat release per volume. The slight differences with variation in argon mole fraction are thought to be due to slight changes in the thermodynamic and chemical properties of the mixtures, including heat capacity, specific heat ratio, and reaction heat, with a change in the argon mole fraction.

In Figs. 8 and 9, the ratios of *re-evaluated* reflection point distance to the channel width, l_r/l_c, are plotted against the argon mole fraction y_{Ar} for the ethylene mixtures (E1–E4) and acetylene mixtures (A1–A2), respectively. The circles and squares correspond to supercritical diffraction in the ethylene and acetylene mixtures, respectively. The closed and open symbols refer to the cases where channel width l_c = 10 and 20 mm, respectively. The reflection point distance l_r was re-evaluated by using the fitted curves shown in Figs. 5 and 6, which represent functional relationships between the reflection point distance and the initial partial pressure of fuel. That is, for a given initial partial pressure of fuel, each data point is given through a calculation using the corresponding fitted curve. Note that data points were given also for the subcritical cases at relatively low initial pressures, where re-initiation does not occur in reality, by extrapolation from data at high initial pressures, because ideally, the reflection point distance is suggested to be roughly inversely proportional to the initial pressure as described above.

342 In Figs. 8 and 9, the data points extrapolated for subcritical cases are indicated by ×-mark symbols.

343 When the channel width is decreased gradually under certain mixture conditions, detonation transmission from
344 the channel to unconfined space will fail at some point. Then, that channel width is the critical width for those
345 mixture conditions. Here, by analogy from the cell width, the critical channel width is expected to be generalized
346 by making it a dimensionless quantity with the use of the ideal reflection point distance, which can serve as a
347 characteristic length of the mixture as described above. Thus, in this study, critical condition is given by the ratio of
348 ideal reflection point distance to the channel width, l_r/l_c. Note that the reflection point distance has relatively large
349 values as a characteristic length, and thus the ratio of the reflection point distance to the channel width is more
350 convenient to express the critical condition rather than its inverse, although the critical condition is usually given by
351 dividing the channel size by a characteristic length of detonation such as the cell width.

352 If we assume that the critical conditions $(l_r/l_c)_{crit}$ lie in a range of 3–5, which is shown by a shaded band in Figs.
353 8 and 9, for all the ethylene and acetylene mixtures with different argon mole fractions, the results shown in Figs. 8
354 and 9 are consistent with the assumption because the critical value of the ratio l_r/l_c is thought to exist between the
355 largest value of the ratio l_r/l_c in the supercritical cases and the smallest value of the ratio l_r/l_c in the subcritical cases
356 for each mixture, whether the outcome overlaps or not. As shown in Table 1, the stability of the mixture increases
357 with the argon mole fraction, thus the critical condition may also vary $(l_r/l_c)_{crit}$ with the argon mole fraction.
358 However, the dependence of the critical condition on the stability cannot be deduced clearly only from the results

obtained in this study, although the dependence is potentially small.

In Figs. 10 and 11, the ratios of the channel width to the cell width, l_c/λ, are plotted against the argon mole fraction y_{Ar} for the ethylene mixtures (E1–E4) as well as the acetylene mixtures (A1–A2), respectively. The closed and open symbols refer to the cases where channel width l_c = 10 and 20 mm, respectively. The ×-mark symbols correspond to subcritical diffraction for all the mixtures. As can be seen in Figs. 10 and 11, the critical value for the ratio l_c/λ, which is thought to exist between the smallest value of the ratio l_c/λ in supercritical diffraction and the largest value of the ratio l_c/λ in subcritical diffraction for each mixture, is not universal but dependent on the argon mole fraction, i.e., stability, as has been well known (e.g. [16, 19]). The critical value $(l_c/\lambda)_{crit}$ appears to be greater for a more highly argon diluted mixture. Here, in the cylindrical (two-dimensional) diffraction problem, the critical value of $(l_c/\lambda)_{crit} \sim 1.5$ has been given, e.g., by Liu *et al*. [11], Benedick *et al*. [12], and Thomas et al. [13] for more unstable mixtures like E1 and A1 in this study, and the critical value $(l_c/\lambda)_{crit} \sim 6$ has also been given by Meredith et al. [17] for a mixture with high argon dilution featuring a more regular cellular structure. Additionally, Shepherd *et al*. [14] suggested that for stoichiometric acetylene-oxygen mixtures, the critical value $(l_c/\lambda)_{crit}$ was doubled by the increase in the argon mole fraction from 0% (corresponding to the A1 mixture) to 80% (corresponding to the A2 mixture), although the critical values were obtained in the spherical (three-dimensional) diffraction problem. Hence, as can be confirmed from Figs. 10 and 11, the results obtained in this study are consistent with known correlations.

Note that the flow-fields obtained in the present setup should be regarded as right halves of symmetric flow-fields

in cylindrical diffraction, and the vertical wall of the observation chamber corresponds to the line of symmetry, thus the critical ratios in this study were also halved. It can be also important to point out the difference in the dependence of the critical condition on the argon mole fraction, i.e., stability. Namely, for the scale of the cell width, the critical condition is significantly dependent on the argon mole fraction, and the critical value at y_{Ar} = 75% is about four times the value at y_{Ar} = 0% as shown in Fig. 10, whereas for the scale of the reflection point distance, the critical value at y_{Ar} = 0% is at most five-thirds times the value at y_{Ar} = 75% as shown in Fig. 8. That is, the critical condition given by the reflection point distance may be less sensitive to the stability of the mixture. This suggests that the diffraction problem is not substantially governed by the cellular spacing.

Finally, significant features of the reflection point distance as a characteristic length are elaborated here through comparison with the cell width. As confirmed in previous studies [29, 30, 36], the reflection point distance was roughly proportional to the cell width and was tens of times the cell width, i.e., the reflection point distance has significantly greater values compared to the cell width. This is particularly important in determining the characteristic lengths of detonable mixtures at relatively high initial pressures, which are encountered in practical systems, including pulse and rotating detonation engines. For instance, for non-diluted fuel-oxygen mixtures at initial pressures greater than the atmospheric pressure, cell widths can be often less than millimeters. Additionally, by using special equipment—such as the apparatus in this study—the reflection point distance may be less cumbersome to determine than the cell width, owing to avoidance of careful preparation of soot foil and

problematic interpretation of the pattern recorded on the foil. It should be also noted that the reflection point distance reflects effects of the three-dimensional cellular structure of the detonation wave because the reflection distance strongly depends on timing of the re-initiation, which again depends on the cellular structure. Here, the usefulness of the cell width is evident in interpreting detonation phenomena, and there exists a huge collection of data. Nevertheless, introduction of the reflection point distance as a characteristic length can still potentially provide a novel point of view. A much wider range of experiments to verify the generality of the reflection point distance parameter is future work.

4. Conclusions

For stoichiometric C_2H_4–O_2 and C_2H_2–O_2 mixtures with or without argon dilution, the processes of detonation diffraction have been investigated in a two-dimensional setup through high-speed schlieren imaging with variations of characteristic length and detonation stability by regulating the initial pressure and argon mole fraction of the mixture. In supercritical cases, reflection point distances of the transverse detonation on the end face of the donor channel were particularly deduced from the obtained sequential schlieren images and analyzed. The reflection point distance can be idealized for the infinitely wide donor channel because of the absence of a length scale characterizing the geometric setup of this problem, and thus it can be a parameter in which properties intrinsic to each detonable mixture are manifested. We draw the following conclusions from our results.

The reflection point distance was roughly inversely proportional to the initial pressure for identical mixtures

411 and independent of the width of the donor channel at high initial pressures. For a certain combination of the fuel

412 and oxidizer, correlations between the reflection point distance and the initial partial pressure of fuel were very

413 similar regardless of the argon mole fraction. Critical conditions of the diffraction problem could be given for the

414 ratio of the reflection point distance to the channel width, and it was suggested that the critical value lies in a range

415 of 3–5 and does not significantly depend on the stability of the mixture.

416

References

[1] Lee, J.H.S.: On the critical diameter problem. In: Bowen, J.R. (ed.) Dynamics of Exothermicity, Gordon and Breach Publishers, Netherlands, pp. 321–335 (1996)

[2] Lee, J.H.S.: The Detonation Phenomena. Cambridge University Press, New York (2008)

[3] Zel'dovich, Y.B., Kogarko, S.M., Simonov, N.N.: An experimental investigation of spherical detonation in gases. Sov. Phys. Tech. Phys. 1, 1689–1713 (1957)

[4] Lee, J.H.S.: Dynamic parameter of gaseous detonations. Ann. Rev. Fluid Mech. 16, 311–336 (1984) https://doi.org/10.1146/annurev.fl.16.010184.001523

[5] Matsui, H., Lee, J.H.: On the measure of the relative detonation hazards of gaseous fuel-oxygen and air-mixtures. Symp. (Int.) Combust. 17, 1269–1280 (1978) https://doi.org/10.1016/S0082-0784(79)80120-4

[6] Mitrofanov, V.V., Soloukhin, R.I.: The diffraction of multi-front detonation waves. Sov. Phys. Dokl. 9, 1055–1058 (1965)

[7] Edwards, D.H., Thomas, G.O., Nettleton, M.A.: The diffraction of a planar detonation wave at an abrupt area change. J. Fluid Mech. 95, 79–96 (1979) https://doi.org/10.1017/S002211207900135X

[8] Edwards, D.H., Thomas, G.O., Nettleton, M.A.: Diffraction of planar detonation in various fuel-oxygen mixtures at an area change. Gasdynamics of Detonations and Explosions, Prog. Astronaut. Aeronaut, AIAA,

75, 341–357 (1981)

https://doi.org/10.2514/4.865497

[9] Moen, I.O., Murray, S.B., Bjerketvedt, D., Rinnan, A., Knystautas, R., Lee, J.H.: Diffraction of detonation initiation from tubes into a large fuel-air explosive cloud. Symp. (Int.) Combust. 19, 635–645 (1982)

https://doi.org/10.1016/S0082-0784(82)80238-5

[10] Knystautas, R., Lee, J.H.S., Guirao, C.M.: The critical tube diameter for detonation failure in hydrocarbon-air mixture. Combust. Flame. 48, 63–83 (1982)

https://doi.org/10.1016/0010-2180(82)90116-X

[11] Liu, Y.K., Lee, J.H., Knystautas, R.: Effect of geometry on the transmission of detonation through an orifice. Combust. Flame. 56, 215-225 (1984)

https://doi.org/10.1016/0010-2180(84)90038-5

[12] Benedick, W.B., Knystautas, R., Lee, J.H.S.: Large-Scale Experiments on the Transmission of Fuel-Air Detonations from Two-Dimensional Channels. Dynamics of Shock Waves, Explosions, and Detonations, Prog. in Astronaut. Aeronaut., AIAA, 94, 546–555 (1984)

https://doi.org/10.2514/5.9781600865695.0546.0555

[13] Thomas, G.O., Edwards, D.H., Lee, J.H., Knystautas, R., Moen, I.O., Wei, Y.M.: Detonation Diffraction by Divergent Channels. Dynamics of Explosions, Prog. in Astronaut. Aeronaut., AIAA, 106, 144–154 (1986)

https://doi.org/10.2514/5.9781600865800.0144.0154

[14] Shepherd, J.E., Moen, I.O., Murray, S.B., Thibault, P.A.: Analyses of the cellular structure of detonations. Symp. (Int.) Combust. 21, 1649–1658 (1986)

https://doi.org/10.1016/S0082-0784(88)80398-9

[15] Moen, I.O., Sulmistras, A., Thomas, G.O., Bjerketvedt, D., Thibault, P.A.: Influence of cellular regularity on the behavior of gaseous detonations. Dynamics of Explosions, Prog. Astronaut. Aeronaut., AIAA, 106, 220–243 (1986)

https://doi.org/10.2514/5.9781600865800.0220.0243

[16] Desbordes, D., Gauerraud, C., Hamada, L., Presles, H.N.: Failure of the classical dynamic parameters relationships in highly regular cellular detonation systems. Dynamic Aspects of Detonations, Prog. Astronaut. Aeronaut., AIAA, 153, 347–359 (1993)

https://doi.org/10.2514/4.866265

[17] Meredith, J., Ng, H.D., Lee, J.H.: Detonation diffraction from an annular channel. Shock Waves. 20, 449–455 (2010)

https://doi.org/10.1007/s00193-010-0256-0

[18] Arienti, M., Shepherd, J.E.: A Numerical Study of Detonation Diffraction. J. Fluid Mech. 529, 117–146 (2005)

https://doi.org/10.1017/S0022112005003319

[19] Eckett, C.A., Quirk, J.J., Shepherd, J.E.: The role of unsteadiness in direct initiation of gaseous detonations. J. Fluid Mech. 421, 147–183 (2000)

https://doi.org/10.1017/S0022112000001555

[20] Radulescu, M.I., Lee, J.H.S.: The failure mechanism of gaseous detonations: experiments in porous wall tubes. Combust. Flame. 131, 29–46 (2002)

https://doi.org/10.1016/S0010-2180(02)00390-5

[21] Bartlmä, F., Schröder, K.: The Diffraction of a Plane Detonation Wave at a Convex Corner. Combust. Flame. 66, 237–248 (1986).

https://doi.org/10.1016/0010-2180(86)90137-9

[22] Jones, D.A., Kemister, G., Oran, E.S., Sichel, M.: The influence of cellular structure on detonation transmission. Shock Waves. 6, 119–129 (1996)

https://doi.org/10.1007/BF02510992

[23] Pintgen, F., Shepherd, J.E..: Detonation Diffraction in Gases. Combust. Flame. 156, 665–677 (2009)

https://doi.org/10.1016/j.combustflame.2008.09.008

[24] Deiterding, R.: High-resolution numerical simulation and analysis of Mach reflection structures in detonation waves in low-pressure H2–O2–Ar mixtures: a summary of results obtained with the adaptive

mesh refinement framework AMROC. J. Combust. 2011, Article ID 738969 (2011)

http://dx.doi.org/10.1155/2011/738969

[25] Li, J., Ning, J., Kiyanda, C.B., Ng, H.D.: Numerical simulations of cellular detonation diffraction in a stable gaseous mixture. Propul. Power Research. *5*, 177–183 (2016)

https://doi.org/10.1016/j.jppr.2016.07.004

[26] Mehrjoo, N., Zhang, B., Portaro, R., Ng, H.D., Lee, J.H.S.: Response of critical tube diameter phenomenon to small perturbations for gaseous detonations. Shock Waves. 24, 219–229 (2014)

https://doi.org/10.1007/s00193-013-0491-2

[27] Mehrjoo, N., Gao, Y., Kiyanda, C.B., Ng, H.D., Lee, J.H.S.: Effects of porous walled tubes on detonation transmission into unconfined space. Proc. Combust. Insti. 35, 1981–1987 (2015)

https://doi.org/10.1016/j.proci.2014.06.031

[28] Murray, S.B., Lee, J.H.S.: On the transformation of planar detonation to cylindrical detonation. Combust. Flame. 52, 269–289 (1983)

https://doi.org/10.1016/0010-2180(83)90138-4

[29] Nagura, Y., Kasahara, J., Sugiyama, Y., Matsuo, A.: Comprehensive visualization of detonation-diffraction structure and sizes in unstable and stable mixtures. Proc. Combust. Inst. 34, 1949–1956 (2013)

https://doi.org/10.1016/j.proci.2012.07.078

[30] Nagura, Y., Kasahara, J., Matsuo, A.: Multi-frame visualization for detonation wave diffraction. Shock Waves. 26, 645–656 (2016) https://doi.org/10.1007/s00193-016-0663-y

[31] Gordon, S., McBride, B.J.: Computer Program for Calculation Complex Chemical Equilibrium Compositions and Applications – I. Analysis. NASA Reference Publication 1311 (1994)

[32] Gordon, S., McBride, B.J.: Computer Program for Calculation Complex Chemical Equilibrium Compositions and Applications – II. User's Manual and Program Description. NASA Reference Publication 1311 (1996)

[33] Ng, H.D., Higgins, A.J., Kiyanda, C.B., Radulescu, M.I., Lee, J.H.S., Bates, K.R., Nikiforakis, N.: Non-linear dynamics and chaos analysis of one-dimensional pulsating detonations. Combust. Theory. Model. 9, 159–170 (2005) https://doi.org/10.1080/13647830500098357

[34] Browne, S., Ziegler, J., Shepherd, J.E.: Numerical Solution Methods for Shock and Detonation Jump Conditions. GALCIT Report FM2006.006 (Revised) (2015)

[35] Smith, G.P., Golden, D.M., Frenklach, M., Moriarty, N.W., Eiteneer, B., Goldenberg, M., Bowman, C.T., Hanson, R.K., Song, S., Gardiner, Jr., W.C., Lissianski, V.V., Qin, Z.: GRI-Mech 3.0, http://combustion.berkeley.edu/gri-mech/version30/text30.html

[36] Strehlow, R.A.: Gas phase detonations: Recent developments. Combust. Flame. 2, 81–101 (1968)

https://doi.org/10.1016/0010-2180(68)90083-7

[37] Kaneshige, M., Shepherd, J.E.: Detonation database. GALCIT Technical Report FM97-8 (1997)

[38] Strehlow, R.A.: Transverse waves in detonations: II. structure and spacing in H_2-O_2, C_2H_2-O_2, C_2H_4-O_2 and CH_4-O_2 systems. AIAA J. 7(3), 492–496 (1969)

https://doi.org/10.2514/3.5134

[39] Abid, S., Dupre, G., Paillard, C.: Oxidation of gaseous unsymmetrical dimethylhydrazine at high temperatures and detonation of UDMH/O_2 mixtures. Dynamic Aspects of Detonations, Prog. Astronaut. Aeronaut., AIAA, 153, 162–181 (1991)

https://doi.org/10.2514/5.9781600866265.0162.0181

[40] Auffret, Y., Desbordes, D., Presles, H.N. : Detonation structure of C_2H_4-O_2-Ar mixtures at elevated initial temperature. Shock Waves. 9, 107–111 (1999)

https://doi.org/10.1007/s001930050145

[41] Denisov, Y.N., Troshin, Y.K.: Structure of gaseous detonation in tubes. Sov. Phys. Tech. Phys. 5(4), 419–431 (1960)

[42] Manzhalei, V.I., Mitrofanov, V.V., Subbotin, V.A.: Measurement of inhomogeneities of a detonation front in gas mixtures at elevated pressures. Combust. Explos. Shock Waves (USSR). 10(1), 89–95 (1974)

https://doi.org/10.1007/BF01463793

[43] Edwards, D.H., Hooper, G., Morgan, J.M., Thomas, G.O.: The quasi-steady regime in critically initiated detonation waves. J. Phys. D. 11(13), 2103–2117 (1978)

https://doi.org/10.1088/0022-3727/11/15/008

[44] Vasil'ev, A.A., Grigor'ev, V.V.: Critical conditions for gas detonation in sharply expanding channels. Combust. Explos. Shock Waves (USSR). 16(6), 579–585 (1980)

https://doi.org/10.1007/BF00794938

[45] Desbordes, D., Vachon, M.: Critical diameter of diffraction for strong plane detonations. Dynamics of Explosions, Prog. Astronaut. Aeronaut., AIAA, 106, 131–143 (1986)

https://doi.org/10.2514/5.9781600865800.0131.0143

[46] Desbordes, D.: Transmission of overdriven plane detonations: Critical diameter as a function of cell regularity and size. Dynamics of Explosions, Prog. Astronaut. Aeronaut., AIAA, 114, 170–185 (1988)

https://doi.org/10.2514/5.9781600865886.0170.0185

[47] Laberge, S., Knystautas, R., Lee, J.H.S. : Propagation and extinction of detonation waves in tube bundles. Dynamic Aspects of Detonations, Prog. Astronaut. Aeronaut., AIAA, 153, 381–396 (1993)

https://doi.org/10.2514/5.9781600866265.0381.0396

[48] Schultz, E., Shepherd, J.E.: Detonation Diffraction Through a Mixture Gradient. GALCIT Report

554 FM2006.008 (2008)

555 [49] Shepherd, J.E., Schultz, E., Akbar, R.: Detonation Diffraction. Proc. International Symposium on Shock

556 Waves. Imperial College, London, UK, July 18-23, 1999.

557 [50] Gallier, S., Le Palud, F., Pintgen, F., Mével, R., Shepherd, J.E.: Detonation wave diffraction in H_2–O_2–Ar

558 mixtures. Proc. Combust. Inst. 36, 2781–2789 (2017)

559 https://doi.org/10.1016/j.proci.2016.06.090

560

561

Table 1 Experimental conditions and typical mixture characteristics. CJ detonation velocities and stability parameters were calculated using the NASA CEA code [31, 32] and ZND code [34] with GRI-Mech 3.0 [35], respectively, at p_0 = 50 kPa and T_0 = 293 K.

	Mixture	y_{Ar} [%]	l_c [mm]	D_{CJ} [m/s]	χ	λ	Cell data
E1	$C_2H_4 + 3O_2$ / Ar	0	10, 20	2340	26	Eq. 2	[10, 38, 39]
E2		50	10	1940	9.7	Eq. 3	[38, 40]
E3		67	10	1800	6.3	Eq. 4	
E4		75	10	1720	4.9	Eq. 5	[38]
A1	$2C_2H_2 + 5O_2$ / Ar	0	10	2390	28	Eq. 6	[16, 41–48]
A2		80	10	1690	5.9	Eq. 7	[16, 48]

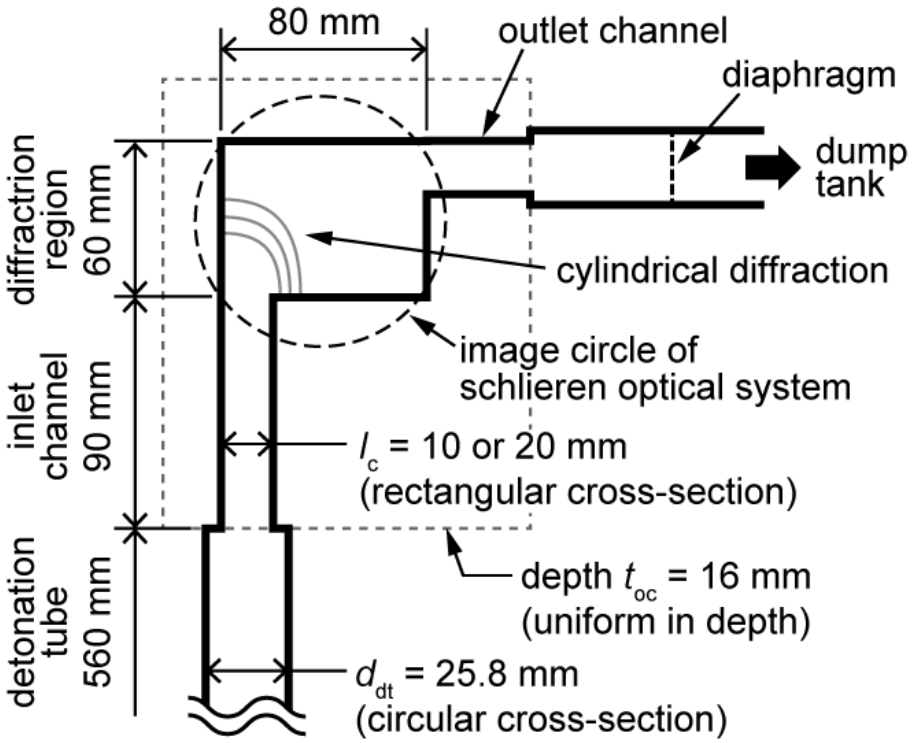

Fig. 1. Schematic of observation chamber.

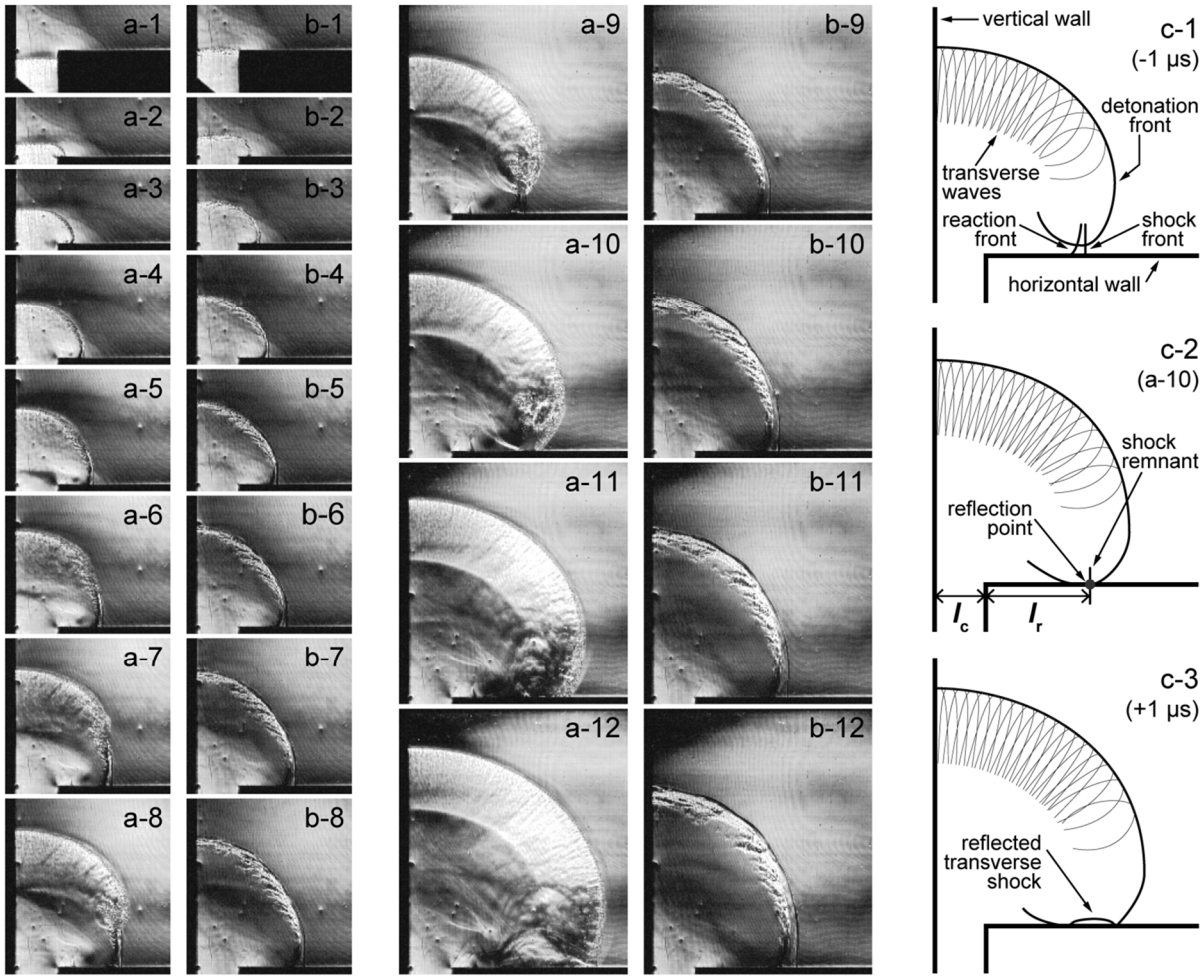

Fig. 2. Typical sequences of single detonation diffraction processes for $C_2H_4 + 3O_2$ (E1) and l_c = 10 mm. (a) Schlieren photographs for supercritical diffraction, p_0 = 30 kPa, T_0 = 20 °C, frame interval = 2 μs. See also Movie 1a, available as supplementary material. (b) Schlieren photographs for subcritical diffraction, p_0 = 10 kPa, T_0 = 20 °C, frame interval = 2 μs. See also Movie 1b, available as supplementary material. (c) Illustration of a reflection event of a transverse detonation wave in supercritical diffraction, frame interval = 1 μs.

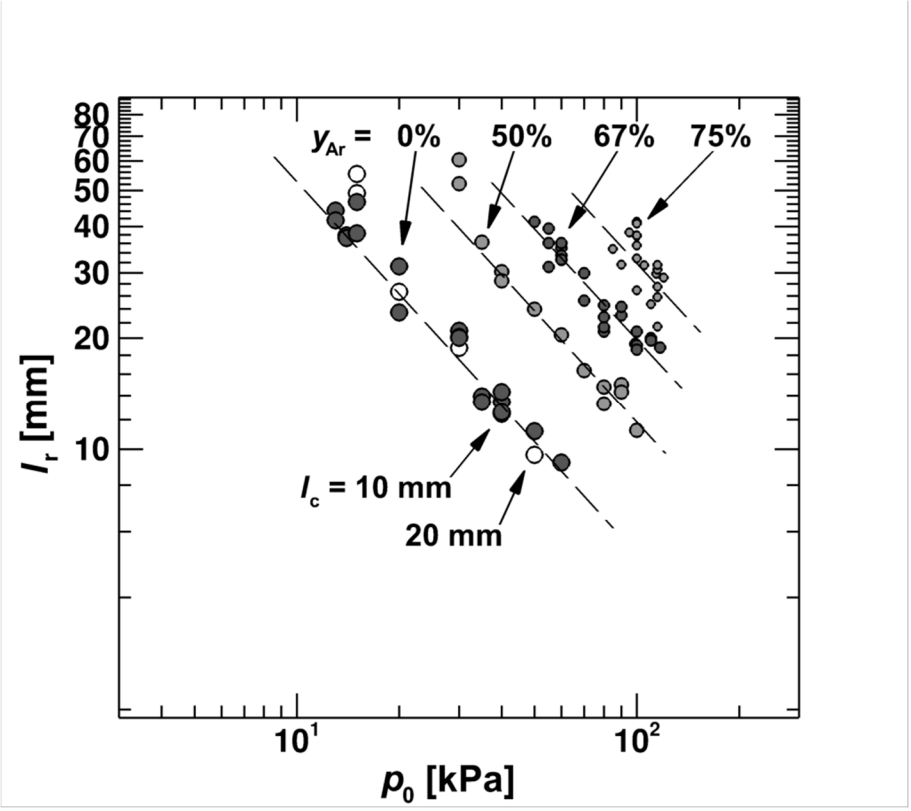

Fig. 3. Reflection point distance vs. initial pressure for supercritical diffraction in ethylene mixtures (E1–E4).

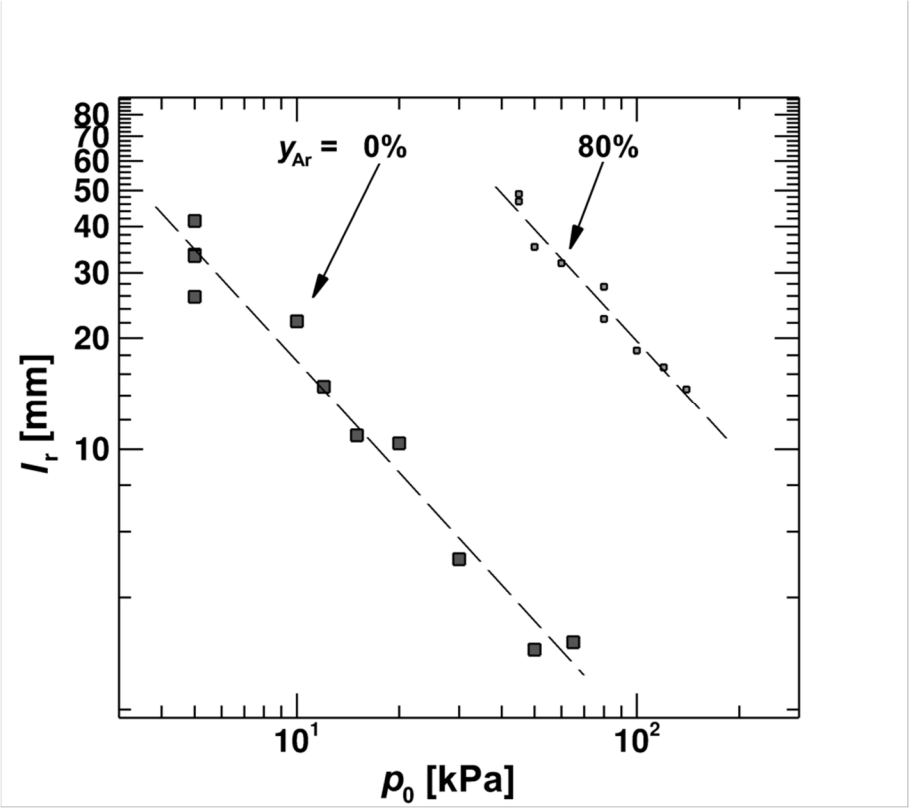

Fig. 4. Reflection point distance vs. initial pressure for supercritical diffraction in acetylene mixtures (A1–A2).

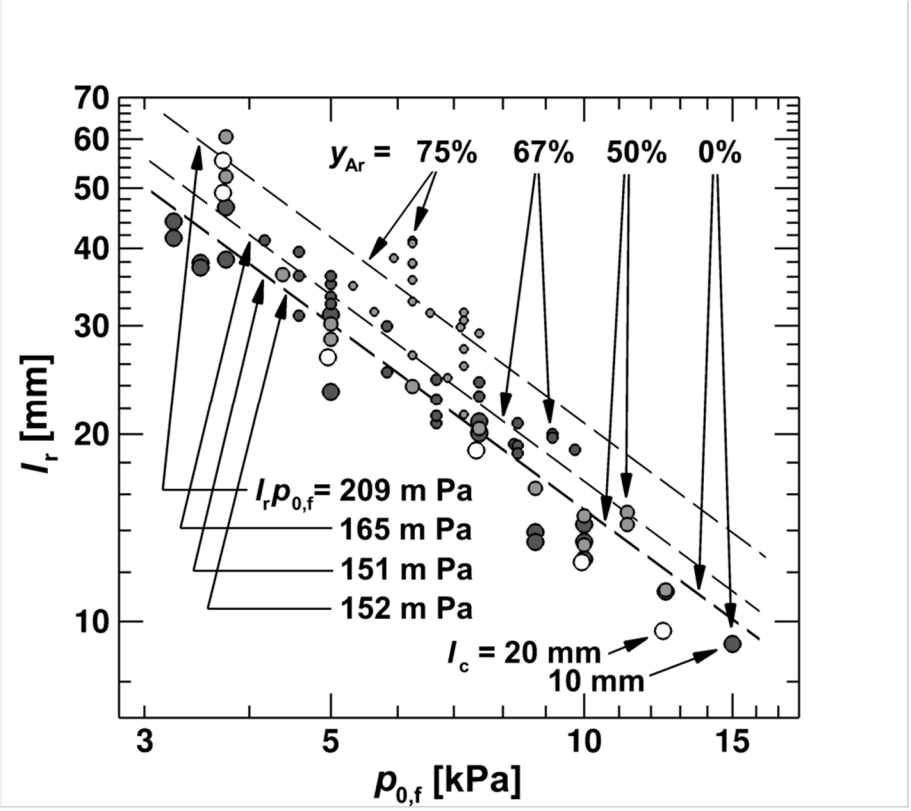

Fig. 5. Reflection point distance vs. initial partial pressure of fuel for supercritical diffraction in ethylene mixtures (E1–E4).

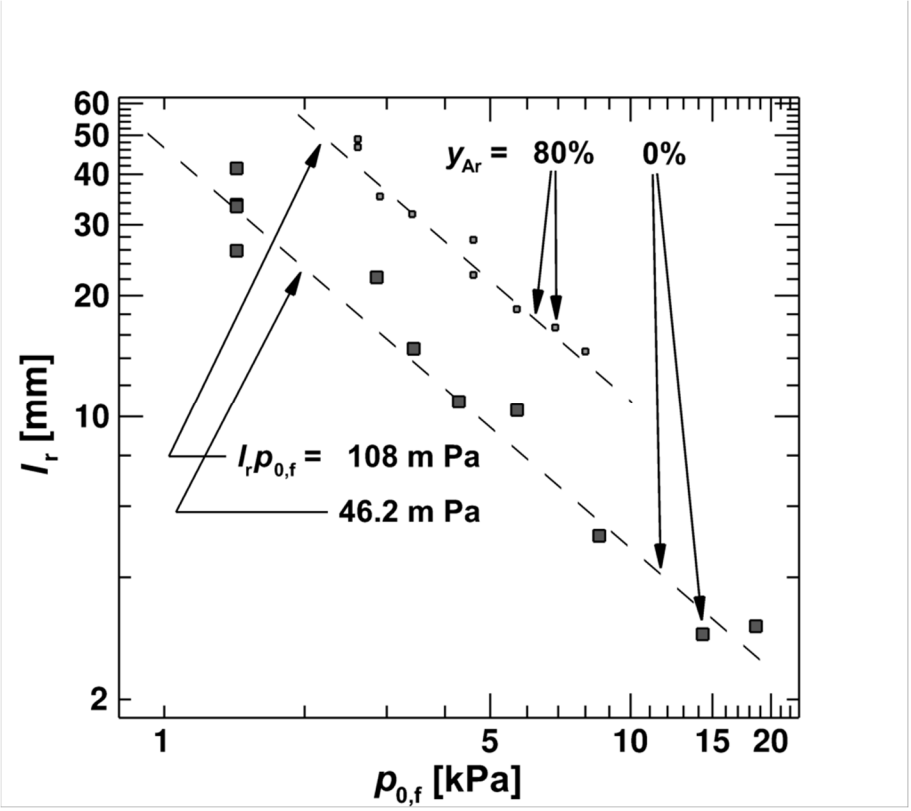

Fig. 6. Reflection point distance vs. initial partial pressure of fuel for supercritical diffraction in acetylene mixtures (A1–A2).

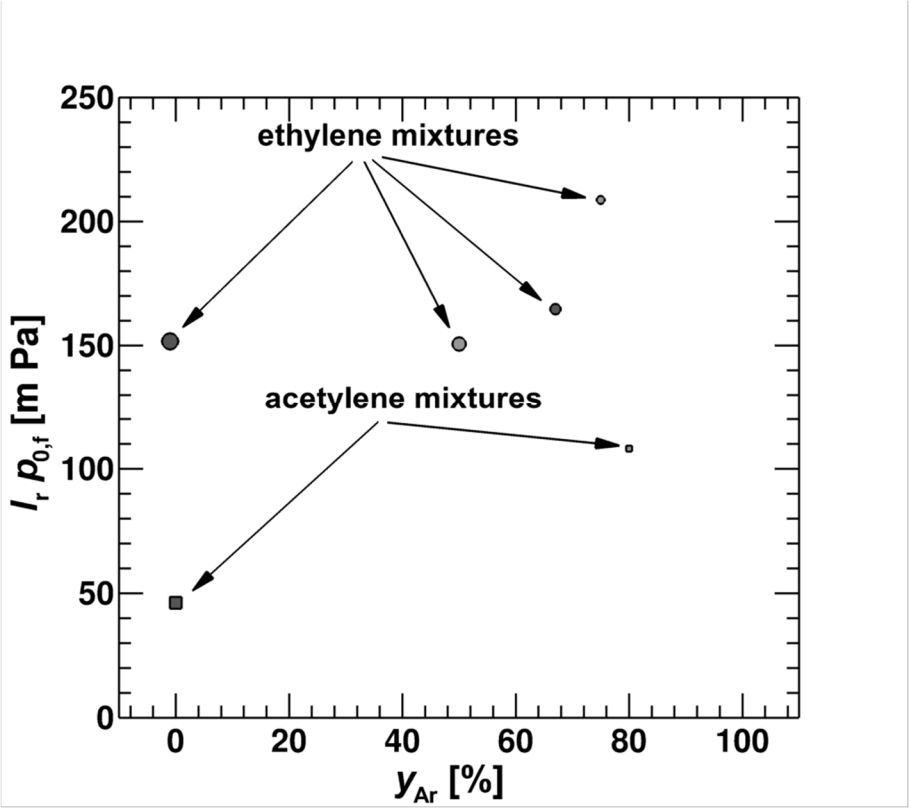

Fig. 7. Product of reflection point distance and initial pressure vs. argon mole fraction for supercritical diffraction.

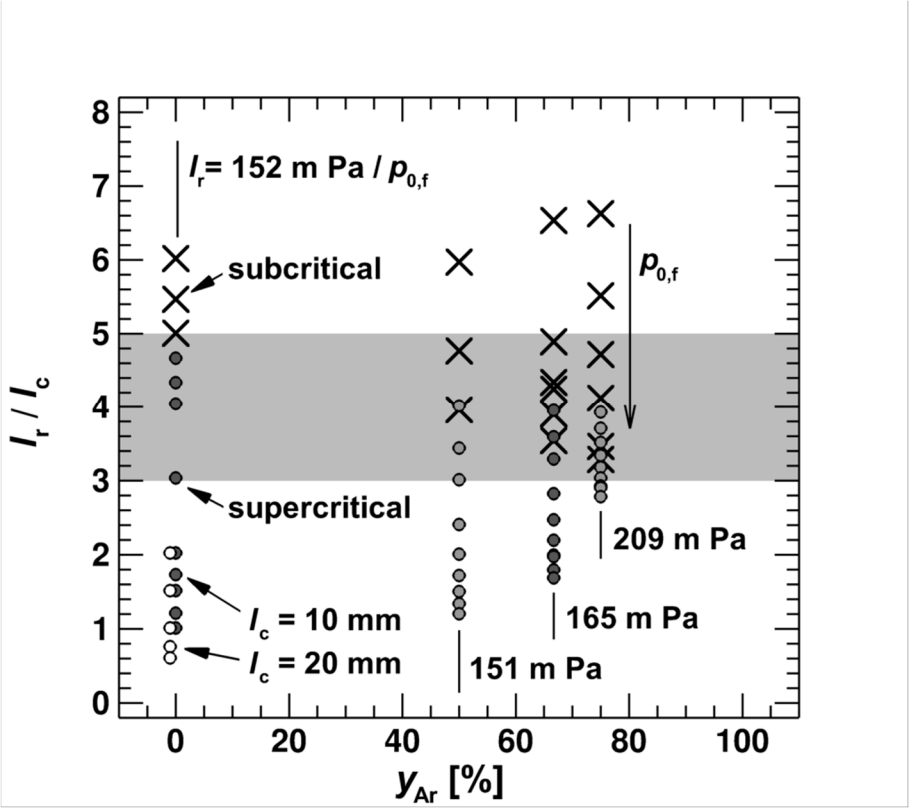

Fig. 8. Ratio of re-evaluated reflection point distance to channel width vs. argon mole fraction in ethylene mixtures (E1–E4). The reflection point distances were re-evaluated by using the fitted curves shown in Fig. 5. For the subcritical diffraction, data points were given by extrapolation.

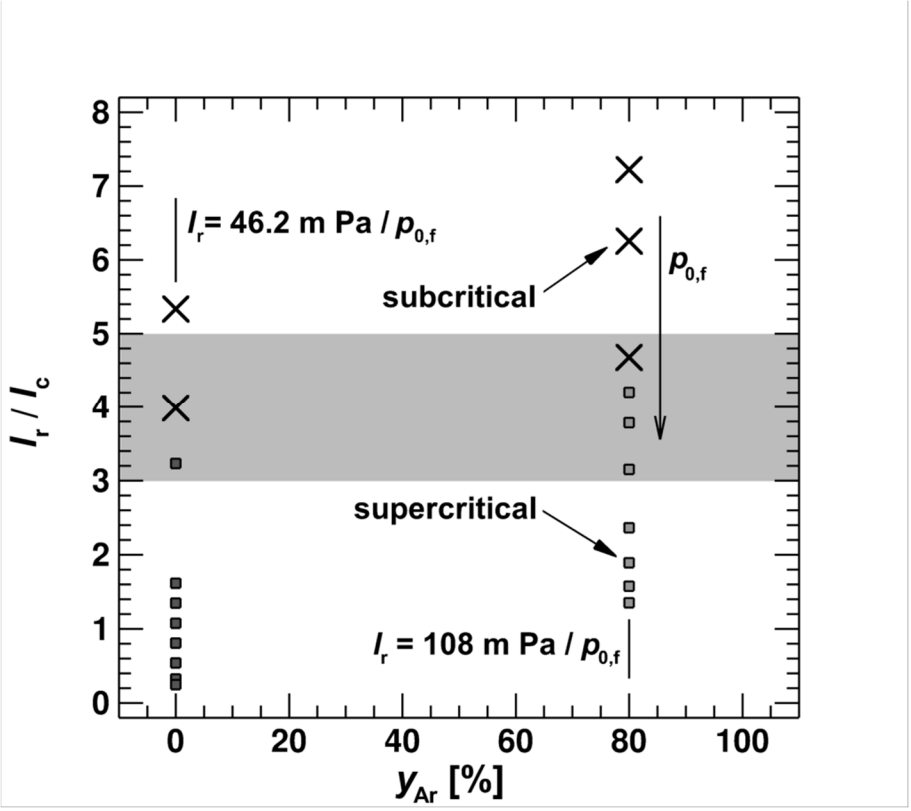

Fig. 9. Ratio of re-evaluated reflection point distance to channel width vs. argon mole fraction in acetylene mixtures (A1–A2). The reflection point distances were re-evaluated by using the fitted curves shown in Fig. 6. For the subcritical diffraction, data points were given by extrapolation.

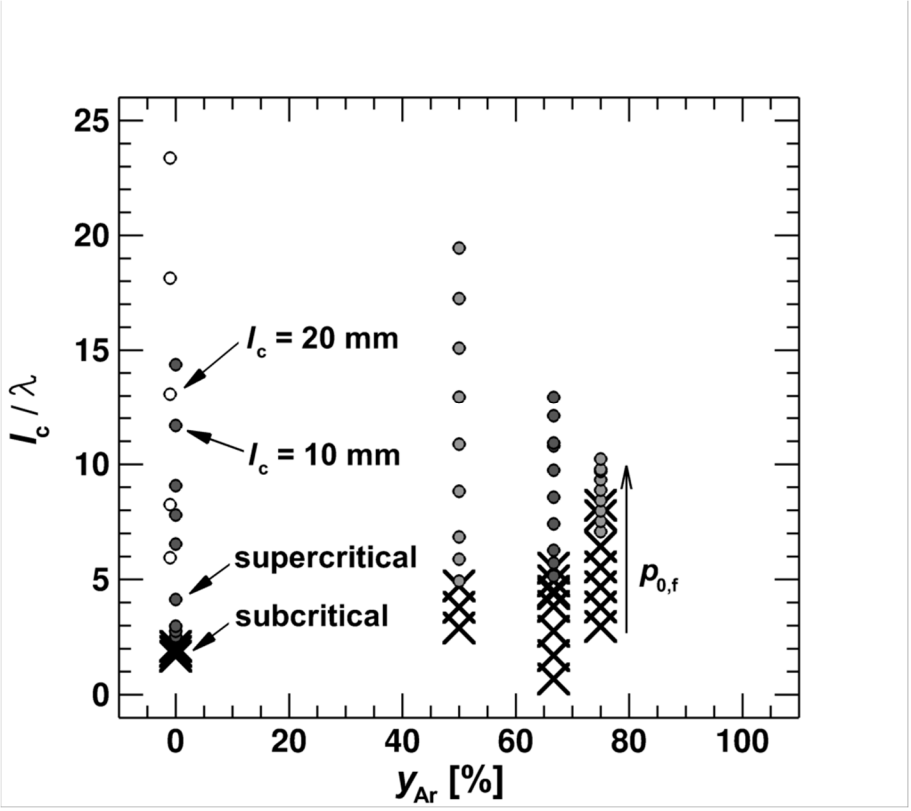

Fig. 10. Ratio of channel width to cell width vs. argon mole fraction in ethylene mixtures (E1–E4).

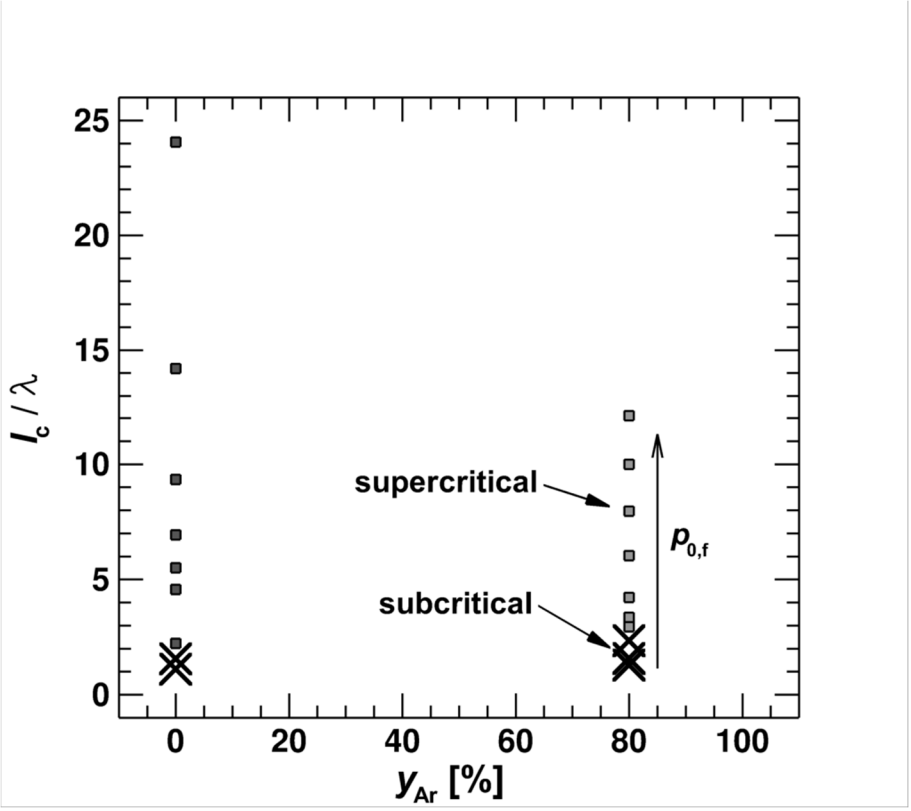

Fig. 11. Ratio of channel width to cell width vs. argon mole fraction in acetylene mixtures (A1–A2).